Intermixing enables strong exchange coupling in nanocomposites: Magnetism through the interfacial ferrite in γ-Fe_{2}O_{3}/NiO

E. Skoropata, T. T. Su, H. Ouyang, J. W. Freeland, and J. van Lierop

Phys. Rev. B **96**, 024447 — Published 28 July 2017

DOI: 10.1103/PhysRevB.96.024447

Intermixing enables strong exchange coupling in nanocomposites: Magnetism through the interfacial ferrite in γ-Fe_2O_3/NiO

E. Skoropata,[1] T. T. Su,[2] H. Ouyang,[2] J. W. Freeland,[3] and J. van Lierop[1]

[1] *Department of Physics and Astronomy, University of Manitoba, Winnipeg, MB, R3T 2N2, Canada**
[2] *Materials Science and Engineering, National Tsing Hua University, Hsinchu, Taiwan*
[3] *Advanced Photon Source, Argonne National Laboratory, Argonne, Illinois 60439, USA*

γ-Fe_2O_3 particles surface modified with NiO crystallites form a unique nanocomposite that points to how to tune strong interfacial exchange coupling. We find that Ni^{2+} migrated into the octahedral sites of the γ-Fe_2O_3 nanoparticle surface, and this $NiFe_2O_4$-like layer permits effective magnetic coupling of Ni and Fe sites that strengthened the interface exchange. A large increase in coercivity coinciding with a loss of exchange bias was achieved by this strong interfacial coupling that resulted in Ni^{2+} moment reversal in the NiO with the γ-Fe_2O_3. This work reveals the importance of intermixing in, and possibility to use, such an exchange coupling regime to alter substantially the coercivity and hence control an important property of exchange coupled nanocomposite magnets.

I. INTRODUCTION

A key property of exchange coupled systems is an interfacial anisotropy that leads to an enhanced coercivity (H_c) and a unidirectional anisotropy that results in exchange bias (i.e. a measured field shift of a hysteresis loop, H_{ex}). The interface magnetism of exchange coupled systems has been a subject of ongoing investigation since the phenomenon was first reported[1] in 1956. Much research has been focused on understanding ferromagnetic(FM)/antiferromagnetic(AF) and ferrimagnetic(FiM)/AF coupled systems to develop a systematic and quantitative description of the interrelationship between the microstructure, intrinsic magnetism of the layers, and exchange bias properties[2–5]. By comparison, less attention has been paid to H_c enhancement resulting from exchange coupling. Previous studies of thin films have revealed that a large H_c enhancement may be obtained in a coupling regime wherein the AF reverses with the FM(FiM)[2,6,7]; a process which necessitates strong interfacial coupling. The relatively recent technological advancements that have enabled observation and characterization of interfacial intermixed layers[8–10] now provide an excellent opportunity to revisit this interesting aspect of exchange coupled magnetism to achieve deeper insight to the physical origin of H_c enhancement. Further, the potential to obtain a large H_c in complex magnetic systems is important to device development and in applications such as nanoparticle-based magnetic hyperthermia and permanent magnets[11].

To address this, we describe the magnetism of γ-Fe_2O_3 nanoparticles surface modified with small NiO particles. The core γ-Fe_2O_3 nanoparticles have disordered surface spins and an H_{ex} due to interactions between the ordered core and disordered surface spin populations[12,13]. Surface modification with the NiO nanoparticles essentially eliminate H_{ex} and the paramagnetic surface spins of the γ-Fe_2O_3, and substantially increase H_c. Using element-specific spectroscopic techniques, we observe the formation of a Ni-ferrite interfacial layer. This layer reduced the disorder at the γ-Fe_2O_3/NiO interface by increasing the coordination of surface atoms. This results in a larger interfacial exchange constant J (vs. the surface J of γ-Fe_2O_3), and enables strong exchange coupling between γ-Fe_2O_3 and NiO. By comparing the atomic Fe relaxation, magnetometry, and susceptometry of γ-Fe_2O_3 and γ-Fe_2O_3/NiO, we find that the H_c enhancement is not a due to a change in the magnetocrystalline anisotropy, K_1, of γ-Fe_2O_3, or due to an increase in the superparamagnetic blocking temperature (T_B), but due to Ni-ion moment reversal in the NiO. Our results demonstrate that interfacial intermixing leads to a strong interfacial exchange coupling (J_{ex}) which can be used to enhance substantially H_c of a nanocomposite system.

II. EXPERIMENTAL METHODS

The γ-Fe_2O_3/NiO nanoparticles were made using a two part seed-mediated synthesis to form γ-Fe_2O_3 cores onto which NiO was deposited. The γ-Fe_2O_3 nanoparticles were synthesized using a thermal decomposition of a Fe-cupferronate precursor, as described in Ref.[14]. To add the NiO, a precursor solution containing 1.8 mmol of Ni-cupferronate in octylamine was heated to 373 K in an argon atmosphere after which 4 mL of the precursor was rapidly injected into 7 mL of γ-Fe_2O_3 nanoparticle solution that had been heated to 523 K in an argon atmosphere. The entire mixture was stirred vigorously at 498 K for 30 minutes, and then stopped by cooling to room temperature. Powder samples used for x-ray diffraction (XRD), Mössbauer spectroscopy, and polarized x-ray experiments were obtained by mixing the nanoparticle stock solution with alcohols to remove excess surfactant, and air drying. Magnetometry and susceptometry experiments were done using samples prepared from 20 μL of nanoparticle stock solution dispersed in 50 mg of paraffin wax to ensure the same particle separation. A transmission electron microscopy (TEM) sample of the nanoparticles was prepared by dropping a mixture of nanoparticle solution diluted in hexanes onto a copper coated carbon grid. TEM images and elemental mapping were collected using a JEOL 2100F.

XRD patterns were collected using a Bruker D8 DaVinci with CuK_α radiation. The structures and lattice parameters were determined using a Rietveld refinement using FullProf[15]. Zero-field cooled (ZFC) and field cooled (FC) *dc*-susceptibilities were measured from 5 K to 300 K using a 0.1 mT applied field with a Quantum Design MPMS XL-5. The *ac*-susceptibility was measured from 5 K to 300 K using a 0.25 mT applied field oscillating at 10 Hz to 1000 Hz. Transmission Mössbauer spectra were collected using a Janis SHI-850 closed cycle refrigeration system and a WissEl constant acceleration spectrometer with a 10-GBq ^{57}Co**Rh** source. The drive velocity was calibrated using α-Fe at room temperature. X-ray absorption spectroscopy (XAS) and x-ray magnetic circular dichroism (XMCD) measurements were done at beamline 4-ID-C of the Advanced Photon Source in a liquid helium cryostat with powder samples mounted on carbon tape onto a cold finger. Spectra were collected over the L_3 and L_2 edges of Fe and Ni. All spectra were collected in total electron yield mode and the XMCD was normalized to the maximum XAS.

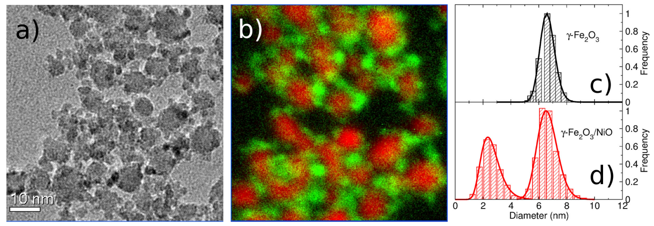

FIG. 1. (a) Transmission electron microscopy (TEM) image of γ-Fe_2O_3/NiO nanoparticles and (b) the elemental map of Fe (red) and Ni (green). Size distribution for (c) γ-Fe_2O_3 and (d) γ-Fe_2O_3/NiO nanoparticles.

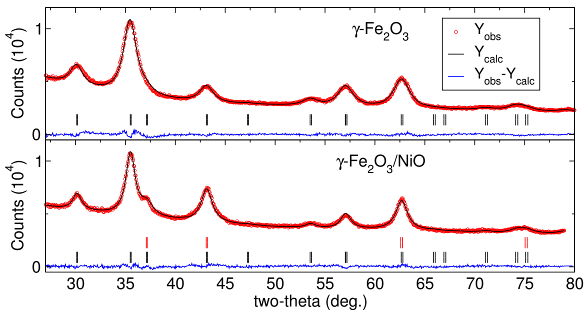

FIG. 2. Powder x-ray diffraction pattern of γ-Fe_2O_3 and γ-Fe_2O_3/NiO nanoparticles, with the results of the refinement (black line) and Bragg markers for the NiO (Fm$\bar{3}$m) (upper red) structure and γ-Fe_2O_3 (Fd$\bar{3}$m) (lower black) structures. The residuals of the refinements are indicated by the solid blue lines.

III. RESULTS AND DISCUSSION

A. Structure and morphology

Transmission electron microscopy images of γ-Fe_2O_3/NiO nanoparticles are shown in Fig. 1a. The size distribution (Fig. 1c-d) obtained from ImageJ[16] analysis of TEM images indicated an average size of 6.61±0.04 nm and distribution width $\ln(\sigma_{D_{TEM}})$=0.05±0.01 for γ-Fe_2O_3 seed particles[17]. For γ-Fe_2O_3/NiO we observe γ-Fe_2O_3 cores with average size 6.52±0.04 nm and $\ln(\sigma_{D_{TEM}})$=0.03±0.01 and additional particles with average size of 2.34±0.03 nm and $\ln(\sigma_{D_{TEM}})$=0.07±0.01. Elemental mapping using electron energy loss spectroscopy (EELS) shown in Fig. 1b identified clearly that small NiO crystallites that formed an incomplete shell on the γ-Fe_2O_3 seeds.

Reitveld refinements[15] of the XRD patterns (Fig. 2) of the nanoparticle systems using the Fd$\bar{3}$m spinel structure of Fe-oxide and the Fm$\bar{3}$m rock-salt structure for the NiO shell indicated a lattice parameter for the spinel phase of 8.380 ± 0.002 Å, typical for γ-Fe_2O_3 or doped-γ-Fe_2O_3 nanoparticles[18]. The rock-salt phase lattice parameter of 4.190 ± 0.002 Å is consistent with NiO[19]. By including Scherrer broadening into the refinements, an average crystallite diameter of the γ-Fe_2O_3 seeds and γ-Fe_2O_3/NiO nanoparticles of 6.5±0.5 nm indicated no change in core size, while a crystallite diameter of ~3 nm was observed for the NiO; all in agreement with the TEM.

B. Magnetometry and Susceptometry

Zero-field-cooled (ZFC) and field-cooled (FC) 10 mT *dc*-susceptibility, $\chi_{dc}(T)$, and 10-1k Hz frequency dependent in-phase and out-of-phase *ac*-susceptibilities ($\chi'_{ac}(\nu,T)$ and $\chi''_{ac}(\nu,T)$, respectively) were used to measure the dynamical responses of the nanoparticles. This range of timescales and fields identifies the different overall responses that reflect the dynamical magnetism of the various spin populations. Shown in Fig. 3a-b, $\chi_{dc}(T)$, for γ-Fe_2O_3 and γ-Fe_2O_3/NiO is quite similar; a maximum ZFC response, and onset of ZFC/FC irreversibility indicate $T_B \sim 75$ K. $\chi'_{ac}(\nu,T)$ (Fig 3c-d) shows a frequency dependent maximum with warming that is preceded by a maximum in $\chi''_{ac}(\nu,T)$ that indicates a maximum of energy dissipation by the nanoparticles' magnetizations occurring just below T_B, and a frequency independent decrease of $\chi'_{ac}(\nu,T)$ for $T > T_B$. A comparison of $\chi_{ac}(\nu,T)$ of the same γ-Fe_2O_3 nanoparticles with a larger interparticle separation (inset of Fig. 3c), indicates some interparticle interactions, however, for the same interparticle separation, there is clearly a much broader range of temperature-dependent response of the γ-Fe_2O_3 cores compared to γ-Fe_2O_3/NiO indicating a change in the dynamics of one or more spin population within

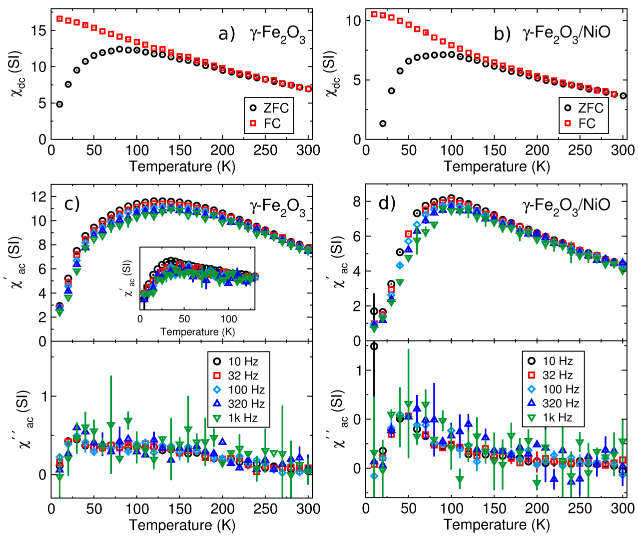

FIG. 3. Zero-field cooled (ZFC) (black ◯) and field-cooled (FC) (red □) *dc*-susceptibility of (a) γ-Fe_2O_3 and (b) γ-Fe_2O_3/NiO nanoparticles. Also shown are the in-phase (top) and out-of-phase (bottom) *ac*-susceptibilities of (c) γ-Fe_2O_3 and (d) γ-Fe_2O_3/NiO nanoparticles prepared using the same interparticle spacing. The inset of (c) shows the same measurement for γ-Fe_2O_3 nanoparticles with a larger interparticle spacing.

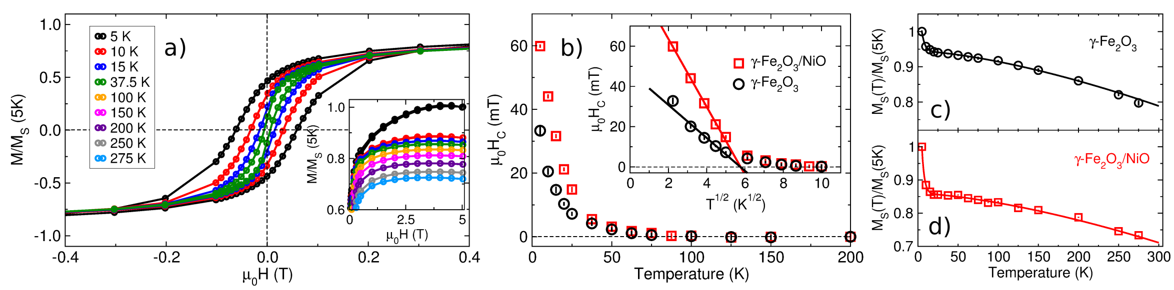

FIG. 4. (a) Typical hysteresis loops for γ-Fe_2O_3/NiO measured from ±5 T after cooling to 5 K in 5 T. The inset shows the temperature variation of the high-field magnetization. b) Temperature dependence of the coercivity, $H_c(T)$, for γ-Fe_2O_3 (red □) and γ-Fe_2O_3/NiO (black ◯). The inset shows $H_c(T^{1/2})$ with the lines indicating a fit as described in the text. Temperature dependence of the saturation magnetization, $M_S(T)$, for (c) γ-Fe_2O_3 and (c) γ-Fe_2O_3/NiO. The solid lines are a fit to a modified Bloch $T^{3/2}$ law as described in the text.

the nanoparticle. By comparison, the γ-Fe_2O_3 and γ-Fe_2O_3/NiO nanoparticles have nearly identical $\chi''_{ac}(\nu,T)$ and $\chi_{dc}(T)$ that indicates comparable $T_B\sim75$ K.

Hysteresis loops measured from 5 K to 300 K after cooling in 5 T present different $H_c(T)$ for γ-Fe_2O_3 and γ-Fe_2O_3/NiO nanoparticles (Fig. 4a-b). The similar T_Bs is reflected in the H_c onset temperature of $T_{B,H_c}\sim75$ K. Interestingly, H_c was nearly doubled with the NiO crystallites (e.g. compare the 5 K values). To first order, $H_c\propto KV/M_s$, where K is the effective anisotropy, V the nanoparticle volume and M_s is the saturation magnetization. Since $H_c(T)$ should be dominated by magnetic relaxation effects, described in the most straightforwards manner by a uniaxial single domain particle[20], $H_c(T)=\frac{2K}{M_s}[1-\sqrt{T/T_B}]$. Fits to this (solid lines in the inset of Fig. 4a) provide an estimate of $K=2.5\times10^4$ J/m^3 for γ-Fe_2O_3 nanoparticles (consistent with previous measurements with an $M_s=3.65\times10^5$ A/m) and $K=5.3\times10^4$ J/m^3 for the γ-Fe_2O_3/NiO nanoparticles. Interestingly, whereas the γ-Fe_2O_3 nanoparticles have $H_{ex}=5.0\pm0.5$ mT at 5 K[21], H_{ex} is nearly eliminated in γ-Fe_2O_3/NiO nanoparticles ($H_{ex}=1.5\pm1$ mT at 5 K). Since the two systems have the same T_B, the changes in H_c and H_{ex} are a result of changes to the surface magnetism of γ-Fe_2O_3, and due to magnetic interactions at the γ-Fe_2O_3/NiO interface. The lack of H_{ex} coinciding with a large H_c enhancement indicates that the unidirecitonal anisotropy was enhanced by strong exchange coupling between the γ-Fe_2O_3 and rotatable AF NiO nanoparticles[2]. A lack of $T_{B,SP}$ enhancement, despite FiM/AF interfacial coupling is due to the $T_{B,SP}\leq75$ K also for the surface NiO crystallites as shown in the supplemental materials[22] (SM), and reported by others for NiO nanoparticles of comparable size[23].

Spin-wave excitations (that can be affected at the nanoscale) and surface disorder alter $M_s(T)$ of a nanoparticle.

We quantified $M_s(T)$ by fitting the high-field region of the loops and verifying the result by extrapolating from $M(\mu_0 H)$ at $1/\mu_0 H$=0. In nanoparticles, $M_s(T)$ is typically described by a Bloch $T^{3/2}$ dependence[24] that is modified to include a term[12,24] $A\exp^{-T/T_f}$ that describes qualitatively the "freezing out" of disordered surface spins that contribute at $\sim T<5T_f$; $M_s(T)=M_0\left[(1-A)(1-BT^{3/2})+A\exp^{-T/T_f}\right]$ where the Bloch constant, $B\propto 1/J$ describes the average exchange strength. Fits to this function (solid lines in Figs. 4c-d) describe $M_s(T)$ well with A=0.21±0.04, T_f=3.3±0.4 K and B=3.19±0.06×10^{-5} K$^{-3/2}$ for γ-Fe_2O_3 nanoparticles, and A=0.42±0.05, T_f=3.2±0.5 K and B=3.31±0.05×10^{-5} K$^{-3/2}$ for γ-Fe_2O_3/NiO nanoparticles. The fit results reveal γ-Fe_2O_3/NiO nanoparticles' disordered surface spin population makes up a larger fraction of the low T M_s while T_f is unaffected. However, reconciling the much lower H_{ex} of the γ-Fe_2O_3/NiO nanoparticles with this result suggests strongly that uncompensated Ni^{2+} spins from the NiO contribute to the low T $M_s(T)$ (e.g. the more pronounced upturn at 5 K). The larger B indicates a weaker overall J amongst spins which contribute to M_s for $T \gg T_f$ (i.e. the "bulk" ordered spins). Stronger exchange interactions are expected between Fe spins at the γ-Fe_2O_3/NiO interface compared to those at the γ-Fe_2O_3 surface due to (better) filled coordination. However, a lower exchange strength compared to the ordered interior spins of the γ-Fe_2O_3 core is expected for coupling through Ni^{2+} (providing a weaker superexchange path compared to Fe^{3+}-O^{2-}-Fe^{3+}) or if some degree of disorder is retained. The larger B for γ-Fe_2O_3/NiO nanoparticles points to the recapture of γ-Fe_2O_3 surface spins, increasing the "effective magnetic volume" via an interfacial population with $J<J_{core}$ but with significantly larger exchange strength compared to J_{surf} of bare γ-Fe_2O_3.

C. Atomic magnetism

Clearly, a better microscopic understanding of the Fe and Ni spin composition and magnetism is necessary to identify the origin of the changes to H_c, H_{ex}, and surface magnetism from the strong exchange coupling enabled by the NiO crystallites. Mössbauer spectroscopy at 10 K ($\ll T_B$ where superparamagnetism does not alter the hyperfine parameters) provides each unique magnetic and electronic environment (site), described by a sextet characterized by a Lorentzian (FWHM) linewidth Γ, hyperfine field B_{hf}, isomer shift δ, and quadrupole splitting Δ, with the relative abundance of each site proportional to the respective spectral areas. The majority of the spectrum of γ-Fe_2O_3/NiO at 10 K is described by components (labeled A and B_I) with hyperfine parameters typical of the B-sites (B_{hf,B_I}=53.32±0.06 T, δ_{B_I}=0.532±0.007 mm/s) and T_d A-sites ($B_{hf,A}$=50.93±0.05 T, δ_A=0.393±0.007 mm/s)[13] with Γ=0.26±0.01 mm/s. Assuming (as usual) that the recoil-free fractions of the A and B-sites are equal at 10 K[26], 30% and 44% is the site abundance of the Fe-ions (versus 62% and 38% for stoichiometric γ-Fe_2O_3). An additional component with $B_{hf,B_{II}}$=49.7±0.1 T, $\delta_{B_{II}}$=0.70±0.03 mm/s and Γ=0.45±0.05 mm/s was necessary to fully describe the spectrum, indicating a change in the environment of some of the Fe-ions occurred after adding the NiO shells, comprising 22% of the Fe-sites. These hyperfine parameters are consistent with the B-sites of non-stoichiometric Ni-ferrite, existing at the interface. The larger δ represents a lower Fe-valence, so that the B_{II}-site is from Fe^{2+}-ions. The lower B_{hf} identifies fewer (or weakened) nearest-neighbour J's, in keeping with the $M_s(T)$ analysis. Also, the v=0, B_{hf}=0 of paramagnetic surface spins[25] of the γ-Fe_2O_3 nanoparticles is not present in the γ-Fe_2O_3/NiO nanoparticles' spectrum, replaced with an interfacial component (observable most clearly as absorption at ∼-3 mm/s) with $B_{hf,int}$=22.1±0.01 T, due to a recapture of the (now) interfacial spins. $B_{hf,int}$ is lower than the ∼50 T of

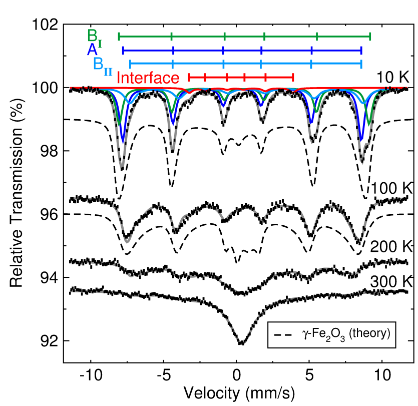

FIG. 5. Mössbauer spectra measured at various temperatures for γ-Fe_2O_3/NiO and the subspectrum component due to individual Fe-sites determined from the 10 K spectrum. Theoretical spectra which well describe the measured spectra for the γ-Fe_2O_3 cores[25] are indicated with a dashed line for comparison.

the core Fe-sites, so the interfacial spin population retained some degree of disorder (likely spin fluctuations). The interfacial Fe-sites also have Δ=0.40±0.05 mm/s due to an asymmetric local electric field that is also observed for the surface spins of γ-Fe_2O_3 (but not in the bulk). This asymmetry in crystal fields about the Fe-ions is suggestive of a larger magnetocrystalline anisotropy at the interface in the nanocomposite system trumping the ∼4% decrease in overall J described above.

Mössbauer spectra measured at 100 K intervals (Fig. 5) aid to identify the nature of the (atomic) spin dynamics in the nanocomposite. The overall temperature dependent spectral collapse that demarks $B_{hf}(T)$ for γ-Fe_2O_3/NiO nanoparticles was comparable to that of the γ-Fe_2O_3 cores[25] (i.e. similar overall line asymmetry and broadening, and B_{hf} reduction with warming). However, the temperature dependence of the spectral lineshape evolution of the γ-Fe_2O_3/NiO system is quite different – much slower spin dynamics at 100 and 200 K (larger spectral components having measurable B_{hf}). These results indicate clearly the impact on the magnetism of the Ni-ferrite interfacial layer from Ni-ions migrating into the surface of the γ-Fe_2O_3 nanoparticles. Bonding between interfacial Fe-ions and Ni-ions strengthens the J_{surf} of γ-Fe_2O_3 and recaptures the (previously) paramagnetic surface spins.

D. Element-specific magnetism

The nature of the Fe- and Ni-sites and their magnetic couplings were further determined from x-ray absorption spectra (XAS) and magnetic dichroic spectra (XMCD) measured over their $L_{2,3}$-edges at 10 K and in ±5 T fields ($\ll T_B$ and M=M_s at 5 T). XAS and XMCD provide valuable insight to the nature of interfacial layers by virtue of the element- and site-specificity, and have been used extensively to study nanostructured magnets[8,21,27–31]. XAS and XMCD spectra were simulated with CTM4XAS[32] using ligand field multiplet calculations of the $2p^63d^n \rightarrow 2p^53d^{n+1}$ transitions for Fe^{3+} and Fe^{2+}, and Ni^{2+}, respectively, and by specifying the crystal field splitting $10Dq$ of O_h and T_d-sites; all sites were described using parameters typical of similar systems[33,34]. Figure 6a-d identifies that the Fe XAS and XMCD spectra were consistent with a spinel Fe-oxide, in agreement with the above Mössbauer results. The XMCD spectrum shows clearly Fe^{2+} and Fe^{3+} O_h-sites whose magnetization aligns parallel to the applied magnetic field, and T_d Fe^{3+}-sites AF superexchange coupled to the O_h-sites. Keeping in mind the preferential surface sensitivity of total electron yield[35] the relative Fe-site abundances of 31% Fe^{2+} O_h, 32% Fe^{3+} T_d, and 37% Fe^{3+} O_h from a best

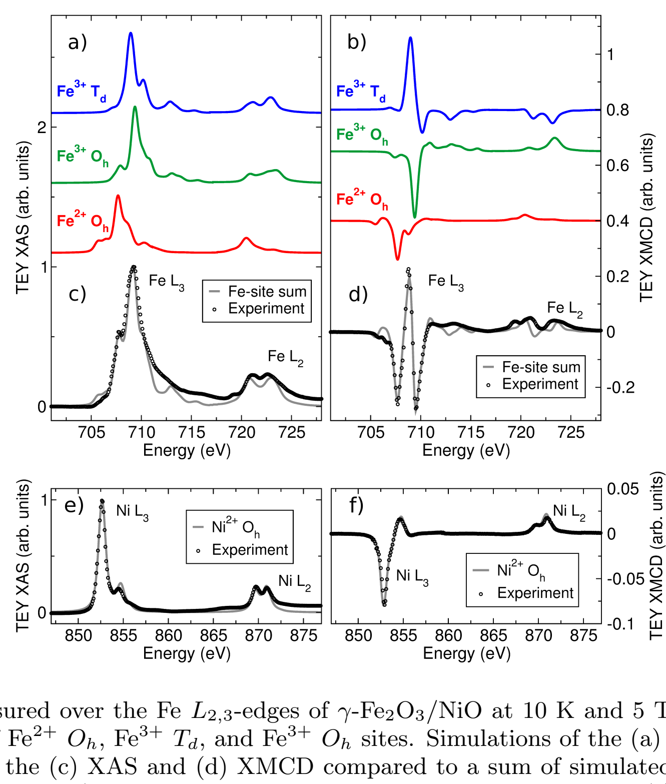

FIG. 6. XAS and XMCD measured over the Fe $L_{2,3}$-edges of γ-Fe_2O_3/NiO at 10 K and 5 T compared with and ligand field multiplet (LFM) simulations of Fe^{2+} O_h, Fe^{3+} T_d, and Fe^{3+} O_h sites. Simulations of the (a) XAS and (b) XMCD of Fe-sites, and measurements (black ∘) of the (c) XAS and (d) XMCD compared to a sum of simulated sites with 31 % Fe^{2+} O_h, 32 % Fe^{3+} T_d, and 37 % Fe^{3+} O_h (grey line) with antiparallel O_h and T_d-site magnetizations. (e) XAS and (f) XMCD measured over the Ni $L_{2,3}$-edges of γ-Fe_2O_3/NiO at 10 K and 5 T compared with and ligand field multiplet (LFM) simulations of Ni^{2+} O_h.

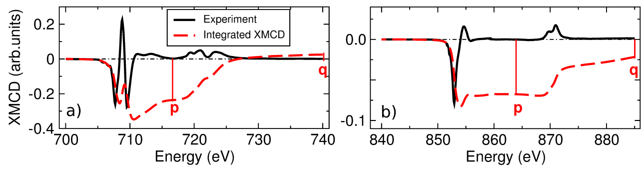

FIG. 7. XMCD of the L_3 and L_2-edges of (a) Fe and (b) Ni for γ-Fe_2O_3/NiO at 10 K and 5 T. The integrated XMCD intensities are shown in dashed lines and p and q are the integrated XMCD of the L_3 and $(L_3 + L_2)$-edges, respectively.

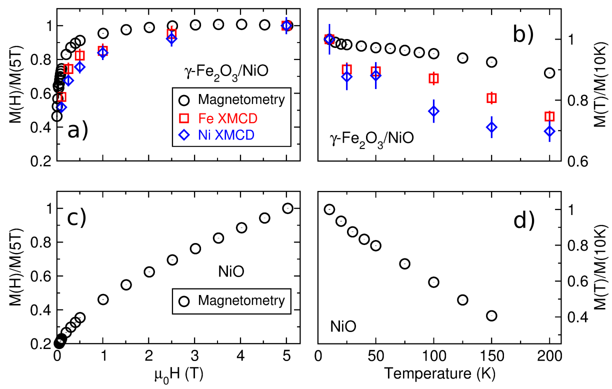

FIG. 8. Temperature (a) and field (b) dependent overall magnetism (◯) obtained from hysteresis loop measurements, and site-specific magnetism of Fe (□) and Ni (⋄) obtained from the L_3-edge XMCD of γ-Fe_2O_3/NiO nanoparticles. Field-dependent measurements were done at 10 K, and temperature dependent measurements were done using 1 T. Also provided is the overall magnetism of $D = 4$ nm NiO nanoparticles including (c) the field-dependent magnetism obtained from hysteresis loop measurement at 10 K and (d) the temperature dependent magnetism in 1 T. Note the difference in scale between (b) and (d).

weighted sum of simulated Fe-sites is in good agreement with the Mössbauer spectral fits, since the larger fraction of Fe^{2+} from XAS and XMCD is a result of the different "surface sensitivity". The Fe XMCD spectra also clearly do not match[36] a pure $NiFe_2O_4$ – in keeping with the γ-Fe_2O_3 core/Ni-ferrite interface/NiO nanocomposite. The Ni XAS and XMCD spectra (Fig. 6e-f) are of O_h Ni^{2+} with a magnetization aligned with the Fe O_h-sites[34,37,38] from the formation of the Ni-ferrite intermixed layer[39,40]. The relatively small Ni^{2+} XMCD signal (compared to $NiFe_2O_4$) is a result of an under-representation of the normalized XMCD from the XAS that speaks to the compensated Ni^{2+} O_h-sites within the AF NiO particles that contribute to the XAS but not the XMCD.

Sum-rules[41–43] were used to obtain the orbit-to-spin moment ratios, $m_\ell/m_s = 2p/(3p - 6q)$, where p and q are the integrated XMCD intensities shown in Fig. 7. For all Fe sites, m_ℓ/m_s=-0.02±0.02, and $m_\ell/m_s = 0.13 \pm 0.02$ for Ni. While there are practical limitations in transition metal-oxide systems[44] to obtaining a precise m_ℓ/m_s ($L_3 - L_2$-edge mixing, sensitivity to data normalization, etc.), the results are consistent with Fe- and Ni-sites of spinel ferrites[34,45].

Field and temperature dependent Fe and Ni L_3 XMCD, shown in Fig. 8, demonstrate a clear coupling of all sites within the intermixed layer, and provide insight to the overall magnetism. $M_{\rm Fe}(T,\mu_0H$=1 T) shows a similar modified Bloch-like behaviour as $M(T)$ from magnetometry. $M_{\rm Ni}(T,\mu_0H$=1 T) from Ni^{2+} is similar to $M_{\rm Fe}(T)$, with a notable difference from the expected behaviour of NiO nanoparticles which have a nearly linear $M(H)$ behaviour and $M(T)$ that varies much more strongly with temperature. This confirms that $M_{\rm Ni}$ is dominated by the sites within the interfacial Ni-ferrite layer. The stronger $M_{\rm Fe}$ and $M_{\rm Ni}$ variation with temperature compared to the overall M from magnetometry is likely due to the previously discussed over-representation of the interfacial layer, and a weakened J compared to that of the interior γ-Fe_2O_3; consistent with the larger B of γ-Fe_2O_3/NiO versus γ-Fe_2O_3, and the results from Mössbauer spectroscopy. While we have identified clearly the existence of the interfacial Ni-ferrite, and the exchange pathways which result in a strong magnetic coupling between the FiM γ-Fe_2O_3 and AF NiO, further measurements using high-resolution TEM in the vicinity of the interface and in-field Mössbauer spectroscopy could shed further light on the atomic-scale structure and magnetism of the interfacial Ni-ferrite.

IV. SUMMARY AND CONCLUSIONS

In summary, we find an increased H_c and decreased H_{ex} of the γ-Fe_2O_3/NiO nanocomposite compared to γ-Fe_2O_3 nanoparticles that reveals strong coupling between the γ-Fe_2O_3 and NiO. This was enabled by an interfacial Ni-ferrite which provided stronger exchange interactions amongst interfacial Fe spins compared to bare γ-Fe_2O_3, that was reflected directly in the partial recapture of the disordered surface spins into the ordered core. We observe clearly that the Ni^{2+} ions are coupled to the B-sublattice of the γ-Fe_2O_3 core, and display temperature and field dependent magnetism expected for a Ni-ferrite with effective Ni-O-Fe exchange pathways that enable strong J_{ex} between the γ-Fe_2O_3 and NiO particles. For a typical system, the properties resulting from exchange coupling depend on K_{FiM} and K_{AF} and the layer volumes V_{FiM} and V_{AF} which determine the energy barrier to the reversal of the layers' magnetization, and the strength of J_{ex}. Usually $K_{FiM}V_{FiM} \ll K_{AF}V_{AF}$, so the AF does not reverse with a field; the non-rotatable pinned AF spins provide the unidirectional anisotropy responsible for H_{ex}. The lack of H_{ex} despite exchange coupling to NiO is due to the low K_{AF} of NiO ($K \sim 4.3\times10^5$ J/m^3)[46] combined with the small NiO particle size – $K_{AF}V_{AF} \sim 2.9\times10^{-21}$ J that is lower than $\sim 3.6\times10^{-21}$ J for γ-Fe_2O_3 core. Thus, the AF NiO does not exert sufficient torque on the core, so $H_{ex}=0$. However, when the interfacial coupling is strong ($J_{ex} \gg K_{AF}V_{AF}$) the AF spins rotate with the FiM layer which can increase H_c substantially[2]. The exchange coupling between γ-Fe_2O_3 and NiO through the Ni-ferrite has a strength $J_{ex} \sim 10^{-3}$ J/m^2, accounting for the surface area of γ-Fe_2O_3 in contact with NiO particles. This regime has been observed in thin films[6,7] which have shown a sharp maximum in H_c coinciding with H_{ex} onset with increasing AF layer thickness, pointing to an effective route to control H_c using interface exchange coupling. We have shown that exchange interactions between γ-Fe_2O_3 and NiO which propagate through an interfacial Ni-ferrite provide precisely this coupling regime, which enabled large H_c enhancement. We have further demonstrated that the effective Fe-O-Ni exchange pathways in the interfacial Ni-ferrite are responsible for the strong coupling between γ-Fe_2O_3 and NiO, which is essential to achieve H_c enhancement.

ACKNOWLEDGMENTS

The authors thank NSERC and CFI of Canada, and NSC of Taiwan. Use of the Advanced Photon Source at Argonne National Laboratories was supported by the US DOE under contract DE-AC02-06CH11357. The authors also thank Dr. Shen-Chuan Lo of the Material and Chemical Research Laboratories, Industrial Technology Research Institute, Taiwan for his assistance with the TEM measurements.

---

[*] umskoroe@myumanitoba.ca;Johan.van.Lierop@umanitoba.ca
[1] W. H. Meiklejohn and C. P. Bean, Phys. Rev. **102**, 1413 (1956).
[2] J. Nogués and I. K. Schuller, J. Magn. Magn. Mater. **192**, 203 (1999).
[3] R. L. Stamps, J. Phys. D: Appl. Phys. **33**, R247 (2000).
[4] M. Kiwi, J. Magn. Magn. Mater. **234**, 584 (2001).
[5] O. Iglesias, A. Labarta, and X. Batlle, J. Nanosci. Nanotechnol. **8**, 2761 (2008).
[6] R. Jungblut, R. Coehoorn, M. T. Johnson, J. aan de Stegge, and A. Reinders, J. Appl. Phys. **75**, 6659 (1994).
[7] H. Xi and R. M. White, Phys. Rev. B **61**, 80 (2000).
[8] H. Ohldag, T. J. Regan, J. Stöhr, A. Scholl, F. Nolting, J. Lüning, C. Stamm, S. Anders, and R. L. White, Phys. Rev. Lett. **87**, 247201 (2001).
[9] S. Estradé, L. Yedra, A. López-Ortega, M. Estrader, M. B. G. Salazar-Alvarez, J. Nogués, and F. Peiró, Micron **43**, 30 (2012).
[10] K. L. Krycka, J. A. Borchers, G. Salazar-Alvarez, A. López-Ortega, M. Estrader, S. Estradé, E. Winkler, R. D. Zysler, J. Sort, F. Peiró, M. D. Baró, C.-C. Kao, and J. Nogués, ACS Nano **7**, 921 (2013).
[11] E. Lottini, A. López-Otrega, G. Bertoni, S. Turner, M. Meledina, G. van Tendeloo, C. de Julián Fernández, and C. Sangregorio, Chem. Mater. **28**, 4214 (2016).
[12] T. N. Shendruk, R. D. Desautels, B. W. Southern, and J. van Lierop, Nanotechnology **18**, 455704 (2007).
[13] J. Tuček, R. Zboril, and D. Petridis, J. Nanosci. Nanotechnol. **6**, 926 (2006).
[14] J. Rockenberger, E. C. Scher, and A. P. Alivisatos, J. Am. Chem. Soc. **121**, 11595 (1999).
[15] J. Rodriguez-Carvajal, Physica B: Condens. Matt. **192**, 55 (1993).
[16] W. S. Rasband, "Image processing and analysis in java," (2005).
[17] R. D. Desautels, E. Skoropata, Y.-Y. Chen, H. Ouyang, J. W. Freeland, and J. van Lierop, J. Phys.: Condens. Matter **24**, 146001 (2012).
[18] R. M. Cornell and U. Schwertmann, *The Iron Oxides: Structure, Properties, Reactions, Occurrences and Uses* (Wiley-VCH Verlag GmbH & Co. KGaA, Weinheim, 2003).

[19] S. Sasaki, K. Fujino, and Y. Takeuchi, Proc. Jpn. Acad. **55**, 43 (1979).
[20] E. F. Kneller and F. E. Luborsky, J. Appl. Phys. **34**, 656 (1963).
[21] E. Skoropata, R. D. Desautels, C.-C. Chi, H. Ouyang, J. W. Freeland, and J. van Lierop, Phys. Rev. B **89**, 024410 (2014).
[22] See Supplemental material at [URL inserted by publisher] for a description of the NiO nanoparticle synthesis and characteriation with x-ray diffraction, *ac*- and *dc*-susceptometry, and hysteresis loop measurements.
[23] E. Winkler, R. D. Zysler, M. Vasquez Mansilla, D. Fiorani, D. Rinaldi, M. Vasilakaki, and K. N. Trohidou, Nanotechnology **19**, 185702 (2008).
[24] R. Aquino, J. Depeyrot, M. H. Sousa, F. A. Tourinho, E. Dubois, and R. Perzynski, Phys. Rev. B **72**, 184435 (2005).
[25] R. D. Desautels, E. Skoropata, and J. van Lierop, J. Appl. Phys. **103**, 07D512 (2008).
[26] G. A. Sawatzky, F. van Der Woude, and A. H. Morrish, Phys. Rev. **183**, 383 (1969).
[27] T. J. Regan, H. Ohldag, C. Stamm, F. Nolting, J. Lünnig, J. Stöhr, and R. L. White, Phys. Rev. B **64**, 214422 (2001).
[28] M. Finazzi, A. Brambilla, L. Dúo, G. Ghiringhelli, M. Portalupi, F. Ciccacci, M. Zacchigna, and M. Zangrando, Phys. Rev. B **70**, 235420 (2004).
[29] A. López-Ortega, M. Estrader, G. Salazar-Alvarez, S. Estradé, I. V. Golosovsky, R. K. Dumas, D. J. Keavney, M. Vasilakaki, K. N. Trohidou, J. Sort, F. Peiró, S. Suriñach, M. D. Baró, and J. Nogués, Nanoscale **4**, 5138 (2012).
[30] A. Juhin, A. López-Ortega, M. Sikora, C. Carvallo, M. Estrader, S. Estradé, F. Peiró, M. D. Baró, P. Sainctavit, P. Glatzel, and J. Nogués, Nanoscale **6**, 11911 (2014).
[31] T. Gaudisson, R. Sayed-Hassan, N. Yaacoub, G. Franceschin, S. Nowak, J.-M. Grèneche, N. Menguy, P. Sainctavit, and S. Ammar, Chrst. Eng. Comm. **18**, 3799 (2016).
[32] E. Stavitski and F. M. F. de Groot, Micron **41**, 687 (2010).
[33] V. S. Coker, C. I. Pearce, R. A. D. Pattrick, G. van Der Laan, N. D. Telling, J. M. Charnock, E. Arenholz, and J. R. LLoyd, Am. Mineral. **93**, 1119 (2008).
[34] G. van der Laan, C. M. B. Henderson, R. A. D. Pattrick, S. S. Dhesi, P. F. Schofield, E. Dudzik, and D. J. Vaughan, Phys. Rev. B **59**, 4314 (1999).
[35] J. Stöhr and H. C. Siegmann, *Magnetism: From fundamentals to nanoscale dynamics* (Springer-Verlag, Berlin Heidelberg, 2006).
[36] S. Matzen, J.-B. Moussy, P. Wei, C. Gatel, J. C. Cezar, M. A. Arrio, P. Sainctavit, and J. S. Moodera, Appl. Phys. Lett. **104**, 182404 (2014).
[37] B. B. Nelson-Cheeseman, R. V. Chopdekar, M. F. Toney, A. Arenholz, and Y. Suzuki, J. Appl. Phys. **111**, 093903 (2012).
[38] J.-B. Moussy, J. Phys. D: Appl. Phys. **46**, 143001 (2013).
[39] G. A. Sawatzky, F. van Der Woude, and A. H. Morrish, Phys. Rev. **187**, 747 (1969).
[40] A. Broese van Groenou, P. F. Bongers, and A. L. Stuyts, Mater. Sci. Eng. **3**, 317 (1969).
[41] B. T. Thole, P. Carra, F. Sette, and G. van der Laan, Phys. Rev. Lett. **68**, 1943 (1992).
[42] P. Carra, B. T. Thole, M. Altarelli, and X. Wang, Phys. Rev. Lett. **70**, 694 (1993).
[43] C. T. Chen, Y. U. Idzerda, H.-J. Lin, N. V. Smith, G. Meigs, E. Chaban, G. H. Ho, E. Pellegrin, and F. Sette, Phys. Rev. Lett. **75**, 152 (1995).
[44] C. Piamonteze, P. Miedema, and F. M. F. De Groot, Phys. Rev. B **80**, 1 (2009).
[45] V. N. Antonov, B. N. Harmon, and A. N. Yaresko, Phys. Rev. B **67**, 024417 (2003).
[46] M. T. Hutchings and E. J. Samuelsen, Phys. Rev. B **6**, 3447 (1972).